Development of a Multi-Objective Optimization Model for the Hard Turning of SKD11 Steel with Nanofluid-Al_2O_3 Minimum Quantity Lubrication Using RSM and PSO

The Vinh Do
Faculty of Mechanical Engineering, Thai Nguyen University of Technology, Thai Nguyen, Vietnam
theinh8880@tnut.edu.vn

Nguyen Anh Vu Le
Faculty of Mechanical Engineering, Nha Trang University, Nha Trang, Vietnam
vulna@ntu.edu.vn (corresponding author)

Received: 7 April 2025 | Revised: 2 May 2025 | Accepted: 24 May 2025

 DOI: https://doi.org/10.48084/etasr.11351

ABSTRACT

This study focuses on the effects of the hard turning of SKD11 steel with nanofluid-based Minimum Quantity Lubrication (MQL) on machining efficiency, optimizing the surface roughness (R_a) and Material Removal Rate (MRR). For this purpose, a hybrid Response Surface Methodology (RSM) and Particle Swarm Optimization (PSO) approach are utilized for the SKD11 hard turning under Al_2O_3 nanofluid-MQL conditions. Initially, 27 experiments were conducted using a Box-Behnken design with Al_2O_3 concentration (0–3% wt), cutting speed (v) of 60–100 m/min, depth of cut (a_p) ranging from 0.2 to 0.6 mm, and feed rate (f) from 0.1 to 0.2 mm/rev, followed by four additional runs, totaling 31 experiments. The resulting RSM models for R_a and MRR achieved high accuracy with an R^2 value of 97.69%. The PSO optimization identified extreme solutions: A minimum R_a of 0.43 µm at 3.0% Al_2O_3, v of 95 m/min, a_p of 0.4 mm, f of 0.12 mm/rev, and a maximum MRR of 9000 mm^3/min at 1.5% Al_2O_3, v of 100 m/min, a_p of 0.6 mm, and f of 0.15 mm/rev. Additionally, a balanced multi-objective solution was obtained at 2.0% Al_2O_3: 98 m/min, 0.5 mm, and 0.14 mm/rev, yielding R_a ≈ 0.55 µm and MRR ≈ 8400 mm^3/min. The proposed RSM-PSO hybrid approach effectively balances surface quality and productivity, outperforming traditional methods. The findings highlight the benefits of iterative refinement and provide practical parameter optimization for the sustainable machining of hardened steels.

Keywords-hard turning; Al_2O_3 nanofluid; MQL; surface roughness; material removal rate; RSM; PSO

I. INTRODUCTION

Hard turning constitutes an effective alternative to traditional grinding, particularly for machining hardened steels, like SKD11. This steel is considered a high-carbon, high-chromium cold work tool steel, widely used in molds, dies, and cutting tools due to its exceptional hardness, wear resistance, and dimensional stability after heat treatment [1]. However, machining SKD11 presents substantial challenges, including excessive tool wear and poor surface integrity, which can degrade the overall performance of the machined components.

To address these challenges, MQL has emerged as a sustainable alternative to conventional flood cooling. MQL significantly reduces cutting fluid consumption while enhancing lubrication and heat dissipation at the tool-workpiece interface [2-4]. However, conventional MQL has limitations in high-speed hard turning due to inadequate cooling efficiency, leading to premature tool wear and compromised surface quality [5]. Moreover, effective mist penetration is difficult to achieve in conventional MQL systems when applied to internal turning operations or complex geometries. The setup becomes more complicated when accounting for accurate nozzle positioning and dedicated atomization equipment. The integration of nanofluids into MQL systems - referred to as nanofluid-MQL - has been proposed in order to overcome these drawbacks.

Nanofluids, which consist of nanoparticles dispersed in base lubricants, significantly enhance the machining performance through mechanisms, such as increased thermal conductivity, improved lubrication, and enhanced load-carrying capacity [6-8]. Compared to conventional MQL, nanofluid-MQL exhibits superior cooling and lubrication properties due to the unique effects of nano-sized solid particles. Specifically, nanoparticles improve the thermal transport efficiency and

introduce key mechanisms. These include the rolling effect, which reduces the friction between the tool and the workpiece, the tribofilm formation, which creates a protective layer on the tool's surface, the self-repairing effect, filling in micro-defects on the workpiece, and the polishing effect, smoothing the machined surface [9-15].

These mechanisms contribute to lower cutting temperatures, reduced friction, and minimized tool wear, thereby enhancing machining efficiency and extending tool life [16, 17]. The nanoparticle concentration parameter has been identified as a crucial factor influencing surface roughness, cutting forces, tool wear, and the overall machining performance. An optimal nanoparticle concentration can reduce surface roughness while maintaining a high MRR [18-20]. Consequently, nanofluid-MQL has been successfully applied in various cutting processes, such as turning, milling, and grinding, proving its effectiveness as a sustainable and high-performance lubrication method [21-26].

Optimization techniques, such as RSM and PSO, have been widely applied in machining research to enhance process efficiency and machining performance. RSM is a powerful statistical tool for developing predictive models and understanding the relationships between the machining parameters and output responses. In addition, PSO inspired by swarm intelligence, finds optimal parameter combinations by improving potential solutions. The integration of these two techniques has gained increasing attention due to their ability to balance accuracy and computational efficiency in machining optimization.

The effectiveness of combining RSM and PSO for optimizing machining parameters has been demonstrated. Authors in [27] compared the RSM-Desirability Approach (DA) with the PSO-Technique for Order Preference by Similarity to Ideal Solution (TOPSIS) in optimizing the finishing turning of 9XC steel under MQL conditions. This combination, revealed that PSO-TOPSIS achieved superior results in both MRR and R_a. Similarly, authors in [28] developed a hybrid NSGA-II and PSO-Neural Network (NN) model to optimize the tool wear, cutting force, and surface roughness in hard turning, demonstrating significant improvements over conventional methods. Moreover, authors in [29] utilized RSM and Artificial Neural Network (ANN) along with a desirability function to optimize the cutting conditions in hard turning, proving that ANN-based models provide higher prediction accuracy. Additionally, a Taguchi-hybrid Quantum PSO algorithm is applied to optimize the CNC turning parameters of the AL7075-T6 aluminum alloy, achieving a superior surface quality compared to the conventional optimization methods [30]. Authors in [31] summarized prediction methods for R_a in finishing machining, including soft computing techniques, such as PSO, ANN, and fuzzy logic.

Despite these advancements, a robust multi-objective optimization framework integrating RSM and PSO remains underexplored, particularly in the hard turning of SKD11 steel using nanofluid-based MQL. This study aims to address this research gap by developing a comprehensive optimization model that considers both R_a minimization and MRR maximization, providing an effective approach for high-performance machining applications.

II. EXPERIMENTAL DETAILS

The experiment evaluates the machining performance of hard turning SKD11 steel under MQL with Al_2O_3 nanofluid, as presented in Figure 1.

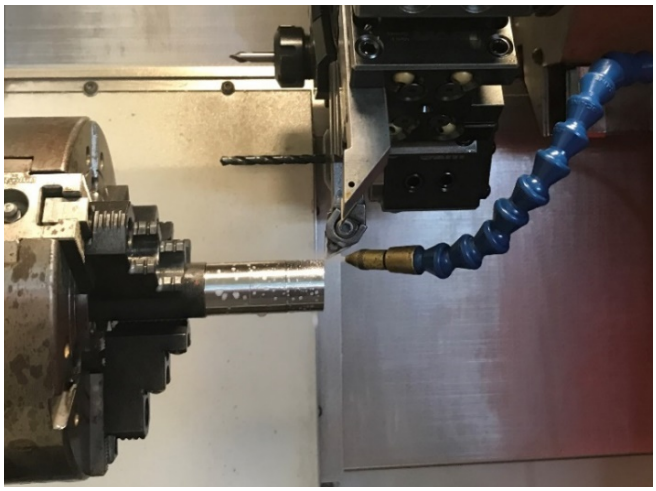

Fig. 1. Experimental setup.

A. Workpiece Material

The workpiece material evaluated in this study is SKD11 tool steel, a high-carbon, high-chromium alloy. The mechanical characteristics of SKD11 combined with high hardness after heat treatment, lead to its frequent use in grinding and hard machining studies [32]. The steel was hardened to 55 HRC through a heat treatment process and subsequently tested using a Mitutoyo Rockwell hardness tester (Model: HR-521) to confirm the desired hardness level. The workpieces were prepared in cylindrical form with a diameter of 40 mm and a length of 200 mm.

B. Machine Tool and Cutting Tool

The turning experiments are performed on an EMCO Maxxturn 45 CNC lathe: A high-precision machine capable of executing complex machining operations with controlled *f* and *v*. The cutting tool used is a Polycrystalline Cubic Boron Nitride (CBN) insert, specifically designed for precision finishing applications on hardened steels (45-65 HRC) and nodular cast iron. The insert has the following specifications: Rhombus configuration with a vertex angle of 35°, insert size: 16 mm, nose radius: 0.4 mm. The cutting tool is rigidly clamped onto a tool holder with a standard negative rake angle, ensuring stable machining conditions.

C. Cutting Conditions and MQL Nanofluid Setup

The experiments are conducted under MQL nanofluid conditions, where Al_2O_3 nanoparticles are dispersed in canola oil to enhance the lubrication and cooling efficiency. To ensure a uniform and stable suspension, the nanofluid is prepared using a magnetic stirrer for 6 h, preventing particle agglomeration and improving its effectiveness in the machining

process. The MQL system operated with a flow rate of 50 mL/h and an air pressure of 4 bar, ensuring a fine mist delivery to the cutting zone.

The cutting parameters and nanoparticle concentration were varied according to a Box-Behnken experimental design, allowing for a comprehensive evaluation of their effects on surface roughness. The Box-Behnken experimental design is selected to model second-order quadratic effects, requiring fewer test runs compared to comprehensive factorial designs. Additionally, it avoids extreme corner points in the design space, which helps mitigate the risk of impractical or detrimental machining conditions. The v, f, and a_p are selected within a predefined range. The Al_2O_3 nanoparticles used in the study have a size of 20 nm, and their concentration in the cutting fluid is adjusted according to the experimental design. By delivering the nanofluid directly to the cutting interface, the MQL system effectively reduced friction and heat generation, thereby enhancing machining performance.

D. Surface Roughness and MRR Measurement

The R_a of the machined surfaces is measured using a Mitutoyo SJ-401 surface roughness tester. Three measurements are taken at different locations along the machined surface and the average value is used for analysis. Each experiment is repeated three times to ensure accuracy and repeatability of the results. The MRR, measured in mm^3/min, is also calculated for each experimental run using:

$$\text{MRR} = v \times f \times a_p \times 1000 \quad (1)$$

where v is the cutting speed, f is the feed rate, and a_p is the depth of cut.

III. EXPERIMENTAL RESULTS AND MODEL DEVELOPMENT

Table I presents the initial experimental design and the corresponding results for the hard turning of SKD11 steel under nanofluid-Al_2O_3 MQL conditions. The experiments were conducted following a Box-Behnken design with 27 runs and four varying input parameters: Al_2O_3 nanoparticle concentration (c), v, m/min), a_p, and f. The levels of these parameters are set as follows: c ranged between 0.0 and 3.0% wt, v from 60 to 100 m/min, a_p from 0.2 to 0.6 mm, and f between 0.10 and 0.20 mm/rev. For each run, R_a and MRR are measured. The R_a values range between 0.43 µm and 1.06 µm, with the minimum observed during experiment No. 26. The MRR values range between 1200 mm^3/min and 9000 mm^3/min, with the maximum recorded during experiments No. 7, No. 17, and No. 25.

Table II presents the Analysis of Variance (ANOVA) results for the initial 27 experiments evaluating the effects of the input parameters on R_a in the hard turning of SKD11 steel under nanofluid-Al_2O_3 MQL conditions. Table II includes sources of variation, Degrees of Freedom (DF), Adjusted Sum of Squares (Adj-SS), Adjusted Mean Squares (Adj-MS), F-values, and p-values for the regression model and its components. The model, with 14 DF, consists of linear terms (c, v, a_p, f), quadratic terms ($c*c$, $v*v$, a_p*a_p, $f*f$), and two-way interaction terms ($c*v$, $c*a_p$, $c*f$, $v*a_p$, $v*f$, a_p*f). The total Adj-SS is 0.631600, with the model accounting for 0.617012 of this variation.

TABLE I. INITIAL BOX-BEHNKEN DESIGN AND RESULTS FOR RA AND MRR.

No.	c (% wt)	v (m/min)	a_p (mm)	f (mm/rev)	R_a (µm)	MRR (mm^3/min)
1	0.0	60	0.2	0.10	0.75	1200
2	0.0	60	0.2	0.20	1.06	2400
3	0.0	60	0.6	0.15	0.92	5400
4	0.0	80	0.4	0.10	0.59	3200
5	0.0	80	0.4	0.20	0.87	6400
6	0.0	100	0.2	0.15	0.77	3000
7	0.0	100	0.6	0.15	0.89	9000
8	0.0	100	0.4	0.10	0.57	4000
9	0.0	100	0.4	0.20	0.85	8000
10	1.5	60	0.4	0.10	0.53	2400
11	1.5	60	0.4	0.20	0.83	4800
12	1.5	80	0.2	0.15	0.65	2400
13	1.5	80	0.6	0.15	0.69	7200
14	1.5	80	0.4	0.10	0.51	3200
15	1.5	80	0.4	0.20	0.81	6400
16	1.5	100	0.2	0.15	0.62	3000
17	1.5	100	0.6	0.15	0.67	9000
18	1.5	100	0.4	0.10	0.49	4000
19	1.5	100	0.4	0.20	0.77	8000
20	3.0	60	0.2	0.15	0.59	1800
21	3.0	60	0.6	0.15	0.65	5400
22	3.0	80	0.4	0.10	0.45	3200
23	3.0	80	0.4	0.20	0.73	6400
24	3.0	100	0.2	0.15	0.55	3000
25	3.0	100	0.6	0.15	0.61	9000
26	3.0	100	0.4	0.10	0.43	4000
27	3.0	100	0.4	0.20	0.69	8000

TABLE II. RA ANOVA RESULTS

Source	DF	Adj-SS	Adj-MS	F-value	p-value
Model	14	0.617012	0.044072	36.25	0.000
Linear	4	0.390901	0.097725	80.39	0.000
c	1	0.090320	0.090320	74.30	0.000
v	1	0.006613	0.006613	5.44	0.038
a_p	1	0.013209	0.013209	10.87	0.006
f	1	0.246533	0.246533	202.80	0.000
Square	4	0.034003	0.008501	6.99	0.004
$c*c$	1	0.002716	0.002716	2.23	0.161
$v*v$	1	0.000243	0.000243	0.20	0.663
a_p*a_p	1	0.009563	0.009563	7.87	0.016
$f*f$	1	0.005370	0.005370	4.42	0.057
2-Way Interaction	6	0.003264	0.000544	0.45	0.833
$c*v$	1	0.000044	0.000044	0.04	0.853
$c*a_p$	1	0.001960	0.001960	1.61	0.228
$c*f$	1	0.000050	0.000050	0.04	0.843
$v*a_p$	1	0.000274	0.000274	0.23	0.643
$v*f$	1	0.000305	0.000305	0.25	0.626
a_p*f	1	0.000007	0.000007	0.01	0.942
Error	12	0.014588	0.001216	-	-
Total	26	0.631600	-	-	-

For the linear terms, f shows the largest effect with an Adj-SS of 0.246533, an F-value of 202.80, and a p-value of 0.000, followed by c, a_p, and v. The F-value, which compares the variance explained by each term to the residual variance, indicates the strength of each factor's influence, with higher values reflecting greater significance. The p-value, representing

the probability of observing such results by chance, is below 0.05 for all linear terms, confirming their statistical significance. Among the quadratic terms, a_p*a_p is significant, while *v***v* and *f***f* present p-values above 0.05, suggesting weaker effects. The two-way interaction terms collectively yield an Adj-SS of 0.003264, an F-value of 0.45, and a p-value of 0.833, with individual terms suggesting no significant contribution due to the low F-values and high p-values. The error term has 12 DF and an Adj-SS of 0.014588, while the overall model exhibits a high F-value of 36.25 and a p-value of 0.000, indicating a robust fit to the data.

Table III summarizes the regression model's performance for predicting surface roughness based on 27 experiments in the hard turning of SKD11 steel under nanofluid-Al_2O_3 MQL conditions. Three statistical metrics are outlined: Standard deviation of the residuals (S), R-squared (R^2), and adjusted R-squared (R^2(adj)). The S value of 0.0348659 indicates the average deviation of the observed R_a values from the predicted values. The R^2 value exhibits that 97.69% of the variability in R_a is adequately explained by the model, suggesting a strong relationship between the input parameters and the response. The R^2(adj) value confirms the model's robustness given its complexity.

TABLE III. REGRESSION MODEL SUMMARY FOR RA

S	R^2 (%)	R^2(adj) (%)	R^2(pred) (%)
0.0348659	97.69	95.00	-

The absence of R^2(pred) during the analysis revealed a critical uncertainty in the model's predictive capability beyond the 27 experiments, despite the favorable S, R^2, and R^2(adj) values. This limitation led to the execution of additional experiments to improve the model's generalizability and reliability for practical use. Consequently, four supplementary runs were conducted, with their details and results presented in Table IV, to refine the model and enhance its predictive accuracy across a broader range of machining conditions.

TABLE IV. ADDITIONAL BOX-BEHNKEN RUNS FOR RA AND MRR

No.	*c* (% wt)	*v* (m/min)	a_p (mm)	*f* (mm/rev)	R_a (µm)	MRR (mm³/min)
28	1.5	90	0.4	0.10	0.51	3600
29	3.0	80	0.4	0.12	0.48	3840
30	0.0	100	0.6	0.15	0.72	9000
31	1.5	80	0.4	0.18	0.68	5760

The ANOVA test results, including the additional four experiments, are presented in Table V. The overall model remains highly significant (F-value = 30.66, P-value = 0.000), with an increased total Adj-SS when compared to previous results, as displayed in Table II, indicating greater variability captured by the 31 experiments. Among the linear terms, *f* retains the strongest influence, followed by *c*, with both showing slightly reduced F-values compared to Table II (202.80 for *f*, 74.30 for *c*). The significance of *v* is higher while the effect of a_p slightly weakens. Regarding the quadratic terms, a_p*a_p remains significant but its contribution is modest, while *c***c*, *v***v*, and *f***f* show no notable significance, consistent with Table II. Two-way interactions remain insignificant with a negligible contribution. The error term receives higher values than during the previous model run (Adj-SS = 0.025250 versus 0.014588), reflecting additional variability from the new runs; yet, lack-of-fit is non-significant (p-value = 1.000), suggesting that the model still fits the data well.

TABLE V. ANOVA RESULTS FOR RA FROM 31 EXPERIMENTS

Source	DF	Adj-SS	Adj-MS	F-Value	p-value	C %
Model	14	0.677324	0.048380	30.66	0.000	96.4
Linear	4	0.431997	0.107999	68.43	0.000	61.5
c	1	0.119449	0.119449	75.69	0.000	17.0
v	1	0.016978	0.016978	10.76	0.005	2.4
a_p	1	0.008731	0.008731	5.53	0.032	1.2
f	1	0.259239	0.259239	164.27	0.000	36.9
Square	4	0.033923	0.008481	5.37	0.006	4.8
c**c	1	0.004021	0.004021	2.55	0.130	0.6
v**v	1	0.000231	0.000231	0.15	0.707	0.0
a_p*a_p	1	0.009262	0.009262	5.87	0.028	1.3
f**f	1	0.003761	0.003761	2.38	0.142	0.5
2-Way Interaction	6	0.003599	0.000600	0.38	0.881	0.5
c**v	1	0.002310	0.002310	1.46	0.244	0.3
c* a_p	1	0.000005	0.000005	0.00	0.957	0.0
c**f	1	0.000200	0.000200	0.13	0.727	0.0
v* a_p	1	0.000085	0.000085	0.05	0.819	0.0
v**f	1	0.000267	0.000267	0.17	0.686	0.0
a_p**f*	1	0.000013	0.000013	0.01	0.929	0.0
Error	16	0.025250	0.001578	-	-	3.6
Lack-of-Fit	15	0.010800	0.000720	0.05	1.000	1.5
Pure	Error	1	0.014450	0.014450	-	-
Total	30	0.702574	-	-	-	-

The key changes from Table II include an enhanced significance of *v*, a slight reduction in the dominance of *f* and a_p, and a higher overall variance (C% = 96.4% for the model), indicating that the additional experiments refined the model's sensitivity to cutting speed while maintaining its robustness. Table VI provides a summary of the regression model's performance for predicting the surface roughness based on 31 experiments.

TABLE VI. MODEL SUMMARY FOR R_a FROM 31 EXPERIMENTS

S	R^2 (%)	R^2(adj) (%)	R^2(pred) (%)
0.0397257	96.41	93.26	81.99

The S value increases slightly to 0.0397257 from 0.0348659 in comparison to Table III, indicating a modest rise in the average deviation of the observed R_a values from predictions due to the additional variability introduced by the new runs. The R^2 value decreases marginally to 96.41% from 97.69%, suggesting that the model explains a slightly lower proportion of the R_a variability with 31 experiments. The R^2(adj) value drops to 93.26% from 95.00%, reflecting a reduction in the model robustness when adjusted for the number of predictors, which is consistent with the increased complexity of the dataset. However, a key improvement is the inclusion of R^2(pred) at 81.99%, which was absent in Table III. This metric, indicating the model's ability to predict new data,

demonstrates that the four additional experiments enabled the assessment of predictive accuracy, addressing a critical limitation of the 27-experiment model and enhancing its practical applicability.

Figure 2 illustrates a probability plot of the residuals used to validate the normality assumption. Most residuals fall along the reference line, indicating that they are an approximately normal distribution. Although one observation deviates slightly, the overall distribution is acceptable and supports the use of the regression model for R_a.

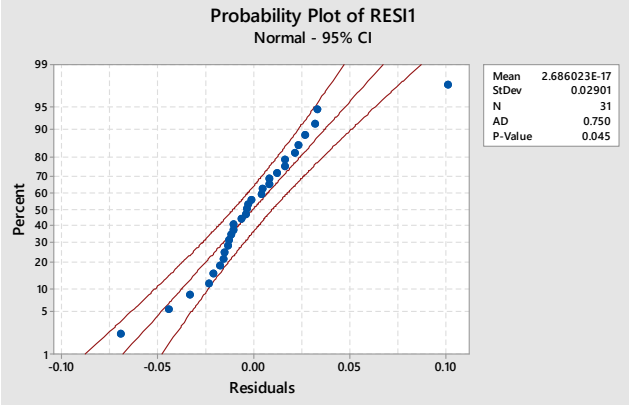

Fig. 2. Normal probability plot of residuals of the Ra regression model.

Performing RSM on the 31-experiment dataset, the regression equations for R_a and MRR are (2) and (3), respectively. The latter capture the relationships between the input parameters (*c, v, a_p, f*) and responses, forming the basis for multi-objective optimization using PSO to balance R_a and MRR:

$$R_a = 1.430 - 0.1281c - 0.00405v - 1.832a_p - 4.68f + 0.01090c^*c + 0.000018v^*v + 2.62a_p{}^*a_p + 27.4f^*f + 0.00514c^*v - 0.0026c^*a_p - 0.066c^*f - 0.00078v^*a_p - 0.0062v^*f - 0.35a_p{}^*f \quad (2)$$

$$\text{MRR} = 3600 - 0.000000c - 60.00v - 9000a_p - -24000f + 0.000000c^*c + 0.000000v^*v - 0.000000a_p{}^*a_p - 0.000000f^*f + 0.000000c^*v - 0.000000c^*a_p + 0.000000c^*f + 150.0v^*a_p + 400.0v^*f + 60000a_p{}^*f \quad (3)$$

To achieve a balanced optimization of the hard turning process for SKD11 steel under nanofluid-Al_2O_3 MQL conditions, PSO is employed. The regression models for R_a and MRR, derived from RSM based on 31 experimental trials, served as the objective functions.

IV. MULTI-OBJECTIVE OPTIMIZATION USING PSO

This section elaborates on the implementation of PSO in Python to achieve multi-objective optimization of R_a and MRR in the hard turning of SKD11 steel under nanofluid-Al_2O_3 MQL conditions. Building on the regression equations (2) and (3) derived from RSM, PSO is employed to identify optimal combinations of *c*, *v*, a_p, and *f* that minimize R_a while maximizing MRR.

The PSO algorithm is implemented using Python with the pyswarm library, adapted for multi-objective optimization. A swarm of 50 particles is initialized within the parameter bounds: *c* (0–3% wt), *v* (60–100 m/min), a_p (0.2–0.6 mm), and *f* (0.1–0.2 mm/rev). The objective functions, based on (2) and (3), are evaluated for each particle. To address the conflicting objectives, a Pareto-based PSO variant is adopted, generating a set of non-dominated solutions forming the Pareto front. The PSO parameters are: inertia weight (*w*) with a value of 0.7, cognitive coefficient (c_1) with a value of 2.0, and social coefficient (c_2) with a value of 2.0, performing 100 iterations for convergence.

The Pareto front reveals trade-offs between R_a and MRR, including extreme solutions yielding a minimum R_a equal to 0.43 µm, with MRR ≈ 5760 mm³/min (*c* = 3.0% wt, *v* = 95 m/min, a_p = 0.4 mm, *f* = 0.12 mm/rev), and a maximum MRR equal to 9000 mm³/min, with Ra ≈ 0.72 µm (*c* = 1.5% wt, *v* = 100 m/min, a_p = 0.6 mm, *f* = 0.15 mm/rev). A balanced multi-objective solution, optimizing both R_a and MRR simultaneously, is identified at *c* = 2.0% wt, *v* = 98 m/min, a_p = 0.5 mm, f = 0.14 mm/rev, resulting in Ra ≈ 0.55 µm and MRR ≈ 8400 mm³/min. This compromise solution offers a practical trade-off, achieving low surface roughness while maintaining high productivity. The RSM-PSO hybrid approach effectively captures these optimal parameter sets, providing flexibility for machining applications tailored to specific requirements.

V. CONCLUSION

This study successfully developed a hybrid Response Surface Methodology (RSM) and Particle Swarm Optimization (PSO) approach to optimize the hard turning process of SKD11 steel under nanofluid-Al_2O_3 MQL conditions. Through an initial 27-experiment Box-Behnken design, supplemented by four additional runs, robust predictive models for surface roughness (R_a) and Material Removal Rate (MRR) were established, achieving an R^2 of 97.69%. The PSO algorithm effectively addressed the multi-objective optimization challenge, identifying a Pareto front of solutions within the parameter bounds (Al_2O_3 concentration (*c*): 0–3% wt, cutting speed (*v*): 60–100 m/min, depth of cut (a_p): 0.2–0.6 mm, feed rate (*f*): 0.1–0.2 mm/rev). The key findings include:

- R_a with minimum value of 0.43 µm at specified conditions: *c*=3.0%, *v*=95 m/min, a_p=0.4 mm, and *f*=0.12 mm/rev.
- MRR maximum value of 9000 mm³/min at specified conditions: *c*=1.5%, *v*=100 m/min, a_p=0.6 mm, and *f*=0.15 mm/rev.
- Balanced solution with Ra≈0.55 µm, MRR≈8400 mm³/min at *c*=2.0%, *v*=98 m/min, a_p=0.5 mm, and *f*=0.14 mm/rev.

These results demonstrate the RSM-PSO hybrid's superiority in balancing surface quality and productivity over traditional methods. The approach provides practical guidance for sustainable machining, with potential for further validation

through the experimental confirmation of the Pareto-optimal solutions.

The current study's findings are consistent with those of several previous studies on nanofluid-assisted MQL machining of hard materials. Authors in [1] reported that optimizing the cutting conditions significantly improved both R_a and MRR in hard turning of SKD11. Similarly, authors in [7, 8] observed an enhanced machining performance in milling SKD11 using SiO_2 nanofluid MQL. The experimental results also align with those reported in [16], where the MoS_2-based MQCL milling of SKD11 was studied and improvements in surface finish and process efficiency were observed. Increasing Al_2O_3 nanoparticle concentration under MQL leads to significant reductions in R_a during THE milling of Hastelloy C276 [24]. Moreover, authors in [18] further investigated the effect of the cutting parameters and MoS_2 nanoparticle concentration in MQL turning, and their findings resulted in trends comparable to those observed in this study.

The present study may serve as a foundation for several future research directions. One possible extension is to investigate the effect of nanoparticle size on the machining performance, as smaller particles may enhance lubrication and cooling behavior due to higher surface area. Furthermore, hybrid nanofluids can be explored by combining two or more types of nanoparticles (e.g., Al_2O_3 + CuO), potentially leveraging the synergistic effects. Additionally, future work could examine the use of different base oils, particularly various types of vegetable oils, to assess their environmental and tribological performance in MQL applications. Finally, validating the current optimization model under industrial-scale cutting conditions would help bridge the gap between laboratory research and practical implementation.

ACKNOWLEDGMENT

The authors gratefully acknowledge the support provided by Thai Nguyen University of Technology while conducting this research.

DATA AVAILABILITY STATEMENT

The data supporting the findings of this study are available from the corresponding author upon reasonable request.

REFERENCES

[1] S. A. Nipu *et al.*, "Turning SKD 11 Hardened Steel: An Experimental Study of Surface Roughness and Material Removal Rate Using Taguchi Method," *Advances in Materials Science and Engineering*, vol. 2023, no. 1, Dec. 2023, Art. no. 6421918, https://doi.org/10.1155/2023/6421918.

[2] Z. Said *et al.*, "A comprehensive review on minimum quantity lubrication (MQL) in machining processes using nano-cutting fluids," *The International Journal of Advanced Manufacturing Technology*, vol. 105, no. 5, pp. 2057–2086, Sep. 2019, https://doi.org/10.1007/s00170-019-04382-x.

[3] D. Li, T. Zhang, T. Zheng, N. Zhao, and Z. Li, "A comprehensive review of minimum quantity lubrication (MQL) machining technology and cutting performance," *The International Journal of Advanced Manufacturing Technology*, vol. 133, no. 5, pp. 2681–2707, Jun. 2024, https://doi.org/10.1007/s00170-024-13902-3.

[4] T.-V. Do and Q.-C. Hsu, "Optimization of Minimum Quantity Lubricant Conditions and Cutting Parameters in Hard Milling of AISI H13 Steel," *Applied Sciences*, vol. 6, no. 3, Mar. 2016, Art. no. 83, https://doi.org/10.3390/app6030083.

[5] B. Shen, Shih ,Albert J., and S. C. and Tung, "Application of Nanofluids in Minimum Quantity Lubrication Grinding," *Tribology Transactions*, vol. 51, no. 6, pp. 730–737, Oct. 2008, https://doi.org/10.1080/10402000802071277.

[6] N. A. C. Sidik, S. Samion, J. Ghaderian, and M. N. A. W. M. Yazid, "Recent progress on the application of nanofluids in minimum quantity lubrication machining: A review," *International Journal of Heat and Mass Transfer*, vol. 108, pp. 79–89, May 2017, https://doi.org/10.1016/j.ijheatmasstransfer.2016.11.105.

[7] G.-T. Bui, T.-V. Do, Q. M. Nguyen, M. H. P. Thi, and M. H. Vu, "Multi-objective optimization for balancing surface roughness and material removal rate in milling hardened SKD11 alloy steel with SIO2 nanofluid MQL," *EUREKA: Physics and Engineering*, no. 2, pp. 157–169, Mar. 2024, https://doi.org/10.21303/2461-4262.2024.003042.

[8] Q.-M. Nguyen and T.-V. Do, "Optimal Approaches for Hard Milling of SKD11 Steel Under MQL Conditions Using SIO2 Nanoparticles," *Advances in Materials Science and Engineering*, vol. 2022, no. 1, Oct. 2022, Art. no. 2627522, https://doi.org/10.1155/2022/2627522.

[9] J. L. Viesca, A. Hernández Battez, R. González, R. Chou, and J. J. Cabello, "Antiwear properties of carbon-coated copper nanoparticles used as an additive to a polyalphaolefin," *Tribology International*, vol. 44, no. 7–8, pp. 829–833, Jul. 2011, https://doi.org/10.1016/j.triboint.2011.02.006.

[10] M.-J. Kao and C.-R. Lin, "Evaluating the role of spherical titanium oxide nanoparticles in reducing friction between two pieces of cast iron," *Journal of Alloys and Compounds*, vol. 483, no. 1–2, pp. 456–459, Aug. 2009, https://doi.org/10.1016/j.jallcom.2008.07.223.

[11] F. Chin˜as-Castillo and H. A. Spikes, "Mechanism of Action of Colloidal Solid Dispersions," *Journal of Tribology*, vol. 125, no. 3, pp. 552–557, Jun. 2003, https://doi.org/10.1115/1.1537752.

[12] L. Wu, Y. Zhang, G. Yang, S. Zhang, L. Yu, and P. Zhang, "Tribological properties of oleic acid-modified zinc oxide nanoparticles as the lubricant additive in poly-alpha olefin and diisooctyl sebacate base oils," *RSC Advances*, vol. 6, no. 74, pp. 69836–69844, Jul. 2016, https://doi.org/DOI https://doi.org/10.1039/C6RA10042B.

[13] X. L. Wang, Y. L. Yin, G. N. Zhang, W. Y. Wang, and K. K. Zhao, "Study on Antiwear and Repairing Performances about Mass of Nano-copper Lubricating Additives to 45 Steel," *Physics Procedia*, vol. 50, pp. 466–472, Jan. 2013, https://doi.org/10.1016/j.phpro.2013.11.073.

[14] J. Ma, Y. Mo, and M. Bai, "Effect of Ag nanoparticles additive on the tribological behavior of multialkylated cyclopentanes (MACs)," *Wear*, vol. 266, no. 7, pp. 627–631, Mar. 2009, https://doi.org/10.1016/j.wear.2008.08.006.

[15] C. C. Chou and S. H. Lee, "Rheological behavior and tribological performance of a nanodiamond-dispersed lubricant," *Journal of Materials Processing Technology*, vol. 201, no. 1, pp. 542–547, May 2008, https://doi.org/10.1016/j.jmatprotec.2007.11.169.

[16] P. Q. Dong, T. M. Duc, and T. T. Long, "Performance Evaluation of MQCL Hard Milling of SKD 11 Tool Steel Using MoS2 Nanofluid," *Metals*, vol. 9, no. 6, Jun. 2019, Art. no. 658, https://doi.org/10.3390/met9060658.

[17] T. V. Do and T. D. Phan, "Multi-objective optimization of surface roughness and MRR in milling of hardened SKD 11 steel under nanofluid MQL condition," *International Journal of Mechanical Engineering and Robotics Research*, vol. 10, no. 7, pp. 357–362, 2021.

[18] N. M. Tuan, T. B. Ngoc, T. L. Thu, and T. T. Long, "Investigation of the Effects of Nanoparticle Concentration and Cutting Parameters on Surface Roughness in MQL Hard Turning Using MoS2 Nanofluid," *Fluids*, vol. 6, no. 11, Nov. 2021, Art. no. 398, https://doi.org/10.3390/fluids6110398.

[19] T. Mehmood and M. S. Khalil, "Enhancement of Machining Performance of Ti-6Al-4V Alloy Though Nanoparticle-Based Minimum Quantity Lubrication: Insights into Surface Roughness, Material Removal Rate, Temperature, and Tool Wear," *Journal of Manufacturing and Materials Processing*, vol. 8, no. 6, Dec. 2024, Art. no. 293, https://doi.org/10.3390/jmmp8060293.

[20] T. V. Do, M.-T. Nguyen, V. T. Nguyen, M. H. P. Thi, and Q.-M. Nguyen, "Improving Efficiency and Surface Quality in Hard Turning of SKD61 Steel Through Cooling and Cutting Parameter Optimization,"

International Information and Engineering Technology Association, vol. 12, no. 3, pp. 991–998, Mar. 2025, https://doi.org/10.18280/mmep.120325.

[21] A. A. Junankar *et al.*, "A Review: Enhancement of turning process performance by effective utilization of hybrid nanofluid and MQL," *Materials Today: Proceedings*, vol. 38, pp. 44–47, Jan. 2021, https://doi.org/10.1016/j.matpr.2020.05.603.

[22] N. M. Tuan, T. T. Long, and T. B. Ngoc, "Study of Effects of MoS2 Nanofluid MQL Parameters on Cutting Forces and Surface Roughness in Hard Turning Using CBN Insert," *Fluids*, vol. 8, no. 7, Jun. 2023, Art. no. 188, https://doi.org/10.3390/fluids8070188.

[23] A. Edelbi, R. Kumar, A. K. Sahoo, and A. Pandey, "Comparative Machining Performance Investigation of Dual-Nozzle MQL-Assisted ZnO and Al2O3 Nanofluids in Face Milling of Ti–3Al–2.5V Alloys," *Arabian Journal for Science and Engineering*, vol. 48, no. 3, pp. 2969–2993, Jul. 2022, https://doi.org/10.1007/s13369-022-07072-1.

[24] F. Günan, T. Kıvak, Ç. V. Yıldırım, and M. Sarıkaya, "Performance evaluation of MQL with AL2O3 mixed nanofluids prepared at different concentrations in milling of Hastelloy C276 alloy," *Journal of Materials Research and Technology*, vol. 9, no. 5, pp. 10386–10400, Sep. 2020, https://doi.org/10.1016/j.jmrt.2020.07.018.

[25] R. Lal Virdi, S. Singh Chatha, and H. Singh, "Performance Evaluation of Inconel 718 under vegetable oils based nanofluids using Minimum Quantity Lubrication Grinding," *Materials Today: Proceedings*, vol. 33, pp. 1538–1545, Nov. 2020, https://doi.org/10.1016/j.matpr.2020.03.802.

[26] R. L. Virdi, S. S. Chatha, and H. Singh, "Experiment evaluation of grinding properties under Al2O3 nanofluids in minimum quantity lubrication," *Materials Research Express*, vol. 6, no. 9, Jun. 2019, Art. no. 096574, https://doi.org/10.1088/2053-1591/ab301f.

[27] T. D. Nguyen, K. H. Nguyen, and L. N. Ha, "A Comparison of RSM-DA and PSO-TOPSIS in optimizing the Finishing Turning of 9XC Steel under MQL Conditions," *Engineering, Technology & Applied Science Research*, vol. 14, no. 3, pp. 14044–14048, Jun. 2024, https://doi.org/10.48084/etasr.7100.

[28] K. Bouacha and A. Terrab, "Hard turning behavior improvement using NSGA-II and PSO-NN hybrid model," *The International Journal of Advanced Manufacturing Technology*, vol. 86, no. 9, pp. 3527–3546, Feb. 2016, https://doi.org/10.1007/s00170-016-8479-6.

[29] A. Labidi, H. Tebassi, S. Belhadi, R. Khettabi, and M. A. Yallese, "Cutting Conditions Modeling and Optimization in Hard Turning Using RSM, ANN and Desirability Function," *Journal of Failure Analysis and Prevention*, vol. 18, no. 4, pp. 1017–1033, Jun. 2018, https://doi.org/10.1007/s11668-018-0501-x.

[30] W.-J. Chen, C.-K. Huang, Q.-Z. Yang, and Y.-L. Yang, "Optimal prediction and design of surface roughness for cnc turning of al7075-t6 by using the taguchi hybrid qpso algorithm," *Transactions of the Canadian Society for Mechanical Engineering*, vol. 40, no. 5, pp. 883–895, Dec. 2016, https://doi.org/10.1139/tcsme-2016-0072.

[31] V.-L. Trinh, "A Review of the Surface Roughness Prediction Methods in Finishing Machining," *Engineering, Technology & Applied Science Research*, vol. 14, no. 4, pp. 15297–15304, Aug. 2024, https://doi.org/10.48084/etasr.7710.

[32] V.-L. Trinh, N.-T. Tran, and D.-T. Nguyen, "Minimum Surface Roughness Prediction of Grinding SKD11 Steel with the Response Surface Methodology," *Engineering, Technology & Applied Science Research*, vol. 15, no. 2, pp. 21469–21474, Apr. 2025, https://doi.org/10.48084/etasr.10117.